A

	grade 1or 2	grade 3 or 4
PHLDA3 LOH +	10	21
PHLDA3 LOH-	11	3

(p<0.01, Fisher's exact test)

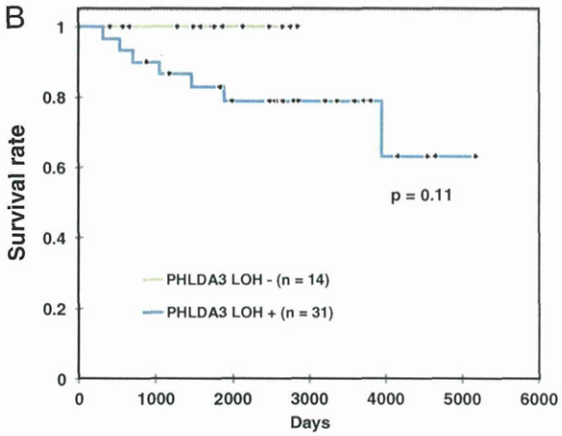

C

	grade 1or 2	grade 3 or 4
MEN1 LOH +	19	19
MEN1 LOH-	4	3

(p=0.73, Fisher's exact test)

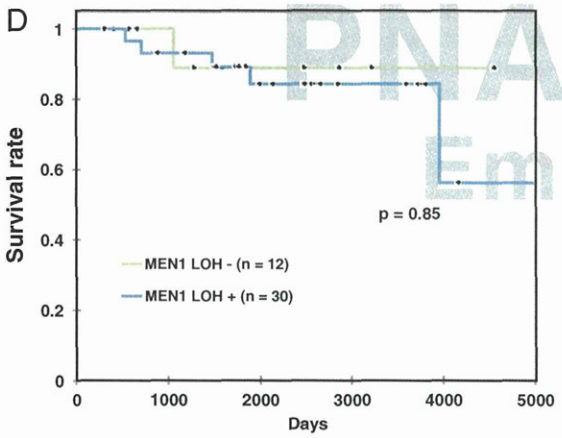

Fig. 3. LOH at the *PHLDA3* and *MEN1* gene locus and progression of PanNETs. (*A*) LOH at the *PHLDA3* gene locus and grade of PanNETs. The *P* value was calculated by Fisher's exact test. (*B*) Kaplan–Meier plots of overall survival of patients with PanNETs. Fourteen or 31 patients without or with *PHLDA3* LOH were analyzed. Wilcoxon test was used to determine the *P* value. (*C*) LOH at the *MEN1* gene locus and grade of PanNETs. (*D*) Kaplan–Meier plot for overall survival of patients with PanNETs. Twelve or 30 patients without or with *MEN1* LOH were analyzed as in *B*.

of DNA methylation levels by methylation-specific PCR revealed detectable methylation only in DLD1 and H1299 cells, cell lines with low *PHLDA3* expression (Fig. 4*D*). It is of note that, in H1299 cells, a human lung NET cell line, *PHLDA3* mRNA expression was remarkably low and methylation was remarkably high. We further treated H1299 cells with 5-aza-C to demethylate the *PHLDA3* gene. As shown in Fig. 4*E*, 5-aza-C treatment resulted in decreased methylation at the *PHLDA3* gene and enhanced expression of *PHLDA3* in a 5-aza-C concentration-dependent manner. A similar result was obtained using a human PanNET cell line A99 (Fig. 4*F*) and the mouse insulinoma cell line MIN6 that has very low PHLDA3 expression (*SI Appendix*, Fig. S3 *A* and *B*). These results indicate that methylation of the *PHLDA3* gene affects *PHLDA3* transcription levels. We then analyzed the methylation status of the *PHLDA3* promoter in PanNET samples that had undergone LOH at the *PHLDA3* locus. As shown in Fig. 4*G*, methylation was not detected in

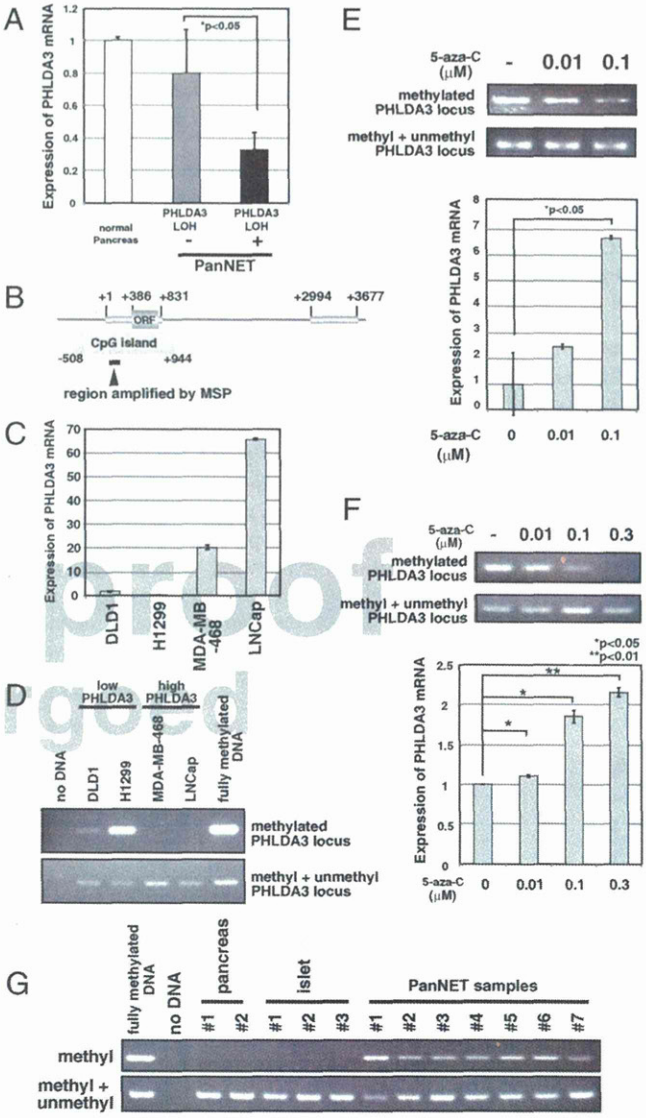

Fig. 4. *PHLDA3* expression and promoter region methylation status in PanNETs. (*A*) *PHLDA3* gene expression in PanNETs. Total RNAs were prepared from normal pancreas and PanNETs. RNA was pooled from 5 normal pancreases for the normal controls. RNA was isolated from PanNET samples with (10 samples) or without LOH (7 samples). Gene expression was quantitated by RT-PCR and normalized to *GAPDH*. (*B*) Genomic organization of *PHLDA3* promoter region and location of CpG island. Wide lines indicate exonic regions of the *PHLDA3* gene (+1 to +831 and +2994 to +3677). (*C*) *PHLDA3* gene expression in cell lines. Gene expression was analyzed as in *A*. (*D*) DNA methylation of the *PHLDA3* promoter. Genomic DNAs from the indicated cell lines were analyzed by methylation-specific PCR. Positions of the primers used in the assay are shown in *B*. Primers designed to amplify methylated DNA (upper panel) or DNA with or without DNA methylation (lower panel) were used. Fully methylated DNA was used as a control. (*E* and *F*) 5-aza-C treatment of Lung NET H1299 cells (*E*) or PanNET A99 cells (*F*). Both genomic DNAs and total RNAs were isolated, and analyzed as in *D* and *A*, respectively. (*G*) Methylation status of *PHLDA3* promoter in normal pancreas, normal isolated islets and PanNETs (samples showing LOH at the *PHLDA3* locus was analyzed). Genomic DNAs were prepared and analyzed as in *D*.

normal pancreas or islets, whereas significant methylation was detected in all LOH+ samples (seven of seven) analyzed. These results show that the *PHLDA3* gene can undergo methylation in addition to LOH in PanNETs, indicating that a two-hit inactivation of the *PHLDA3* gene may often occur. We also analyzed LOH− samples and found detectable levels of methylation in two of four samples (*SI Appendix*, Fig. S4). Thus, the repression of *PHLDA3* expression in LOH− samples due to methylation may also contribute to tumor progression in PanNETs.

PHLDA3 Controls Akt Activity, Cell Proliferation, and Apoptosis of Islet Cells. PanNETs are derived from pancreatic islet endocrine cells. It is well known that, in islet β cells, Akt signaling plays a central role in promoting cell growth and inhibiting apoptosis (5). Therefore, in β cells, loss of PHLDA3 function may result in the hyperactivation of Akt oncogenic signaling, and thus lead to tumor progression. To analyze the function of PHLDA3 in islet β cells, we examined RIN and MIN6 cells, cell lines derived from pancreatic β cells (Fig. 5 *A*–*E*). Whereas RIN cells have detectable levels of PHLDA3 expression, MIN6 has very low PHLDA3 expression (*SI Appendix*, Fig. S3*A*). We first used a gain-of-function approach to confirm that PHLDA3 functions as a repressor of Akt in MIN6 cells. As shown in Fig. 5*A*, expression of PHLDA3 resulted in decreased Akt activation levels and decreased phosphorylation of signaling molecules downstream of Akt. Similar results were obtained using *PHLDA3*$^{-/-}$ mouse embryonic fibroblasts (MEFs, *SI Appendix*, Fig. S5). Next, we knocked down PHLDA3 expression in RIN cells using siRNA against PHLDA3 (Fig. 5 *B* and *C*), and observed increased Akt activation and cell proliferation (Fig. 5 *D* and *E*). We observed similar results in normal primary rat islet cells, i.e., knockdown of PHLDA3 expression resulted in activation of Akt (with or without glucose stimulation) and significant enhancement of cell proliferation (Fig. 5 *F*–*H* and *SI Appendix*, Fig. S6). Next, we analyzed the effect of PHLDA3 expression on the apoptosis of islet cells induced by Streptozotocin (STZ), a chemical that is particularly toxic to insulin-producing β cells (14). We observed that although inhibition of *PHLDA3* expression by siRNA was relatively poor in isolated rat islets (Fig. 5*I*), this knockdown significantly reduced the number of apoptotic cells caused by STZ treatment (Fig. 5*J*). Collectively, these results demonstrate that PHLDA3 controls Akt activity, cell growth, and the apoptosis of islet cells.

Development of Hyperplastic Islets in *PHLDA3*-Deficient Mice. To analyze the effect of PHLDA3 deficiency on islets in vivo, we examined the pancreases of *PHLDA3*-deficient mice. Differences in islet sizes were not detected in 3-mo-old *PHLDA3*$^{+/+}$ or *PHLDA3*$^{-/-}$ mice (*SI Appendix*, Fig. S7). However, in 6-mo-old *PHLDA3*$^{-/-}$ mice, we found significantly fewer islets that were smaller than 0.01 mm^2 and significantly more islets that were larger than 0.01 mm^2, compared with *PHLDA3*$^{+/+}$ mice (Fig. 6 *A* and *C*). However, the overall average islet size at 6 mo was not significantly different between *PHLDA3*$^{+/+}$ and *PHLDA3*$^{-/-}$ mice (Fig. 6*E*). At 10 mo, abnormally large islets (larger than 0.08 mm^2) were frequently found (Fig. 6 *B* and *D*), and the average islet sizes were significantly larger in 10-mo-old *PHLDA3*$^{+/-}$ and *PHLDA3*$^{-/-}$ mice compared with *PHLDA3*$^{+/+}$ mice (Fig. 6*E*). Thus, a difference in islet sizes between *PHLDA3*$^{+/+}$ and *PHLDA3*$^{-/-}$ mice appears to emerge between 3 and 10 mo of age. We stained the islets with Ki67 antibody and found significantly more Ki67-positive cells in *PHLDA3*$^{-/-}$ islets compared with the *PHLDA3*$^{+/+}$ islets (Fig. 6*F*; representative images are shown in *SI Appendix*, Fig. S8). These data show that loss of PHLDA3 expression results in enhanced proliferation of islet cells.

Enhanced Proliferation of β Cells and Altered Glucose Metabolism in *PHLDA3*-Deficient Mice. The islets were further stained with anti-insulin and anti-glucagon antibodies to determine the numbers

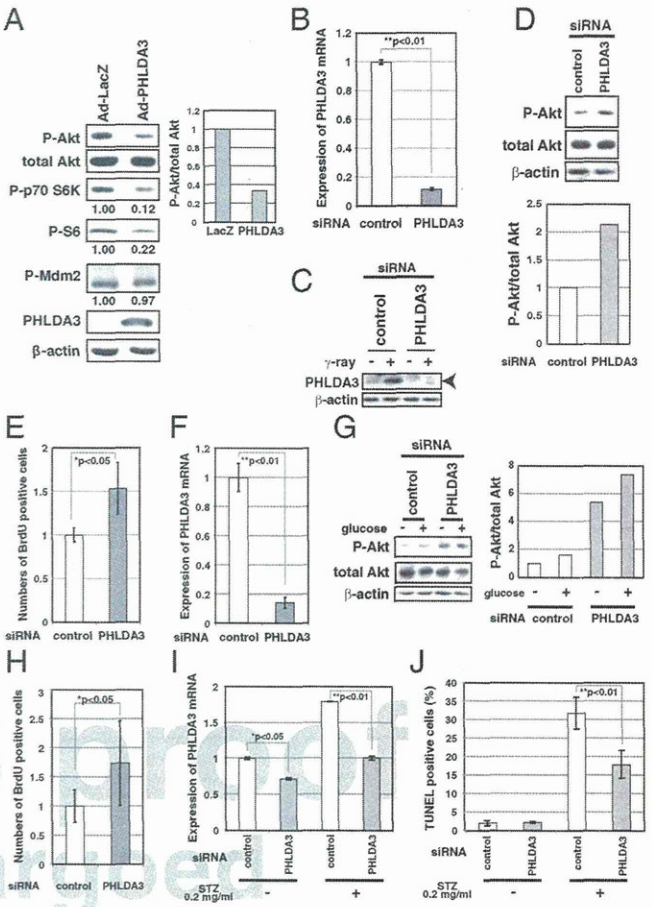

Fig. 5. Effect of PHLDA3 expression on Akt activity, cell proliferation and apoptosis of islet cells. (*A*) Effect of PHLDA3 expression on Akt activity in MIN6 cells. MIN6 cells were transduced with Ad-LacZ or Ad-PHLDA3 at a moi of 35, and harvested 30 h postinfection. Akt activation and phosphorylation of Akt downstream signaling molecules were analyzed by Western blotting and quantified by normalization to total Akt levels (P-Akt) or by β-actin levels (P-p70 S6K, P-S6, P-Mdm2). (*B* and *C*) Efficiency of siRNA inhibition of PHLDA3 expression in RIN cells. RIN cells were transfected with control or PHLDA3 siRNAs. *PHLDA3* mRNA levels were analyzed 31 h posttransfection by quantitative RT-PCR, standardized against β-actin (*B*). PHLDA3 protein levels were also determined 48 h posttransfection by Western blotting (*C*), using cells subjected to γ-ray irradiation (20 Gy) versus untreated. The γ-ray irradiated samples were included to help identify the band representing PHLDA3 protein (PHLDA3 is induced by p53 activation). (*D*) Effect of PHLDA3 expression on Akt activation in RIN cells. RIN cells were transfected as in *B* and Akt activation was analyzed by Western blotting 31 h posttransfection (left) and quantified by normalization to total Akt levels (right). (*E*) Effect of PHLDA3 expression on RIN cell proliferation. RIN cells were transfected as in *B*, and labeled with BrdU for 3 h and harvested 28 h post transfection. BrdU positive cells were quantified by using Ziva Ultrasensitive BrdU assay. (*F*) siRNA suppression of *PHLDA3* expression in primary islet cells. Isolated primary islet cells were transfected with control or PHLDA3 siRNA, harvested 30 h post transfection, and *PHLDA3* mRNA levels were analyzed by quantitative RT-PCR as in *B*. (*G*) Effect of PHLDA3 expression on Akt activation in primary islet cells. Cells were transfected with siRNA as in *F* and 48 h post-transfection were treated with glucose (30 mM) for 20 min. Levels of Akt activation were analyzed as in *D*. (*H*) Effect of PHLDA3 expression on primary islet cell proliferation. Cells were transfected as in *F*, labeled with BrdU for 4 h and harvested 30 h post transfection. BrdU positive cells were analyzed as in *E*. (*I* and *J*) Effect of PHLDA3 expression on STZ-induced apoptosis of primary rat islets. Isolated islets were pooled from three rats, and transfected with control or PHLDA3 siRNA. At 75 h posttransfection, islets were treated with STZ (20 μg/mL) for 30 min. Islets were then cultured overnight, and total RNAs were prepared and *PHLDA3* expression was analyzed by quantitative RT-PCR as in B (*I*), or subjected to TUNEL staining and analyzed by FACS (*J*).

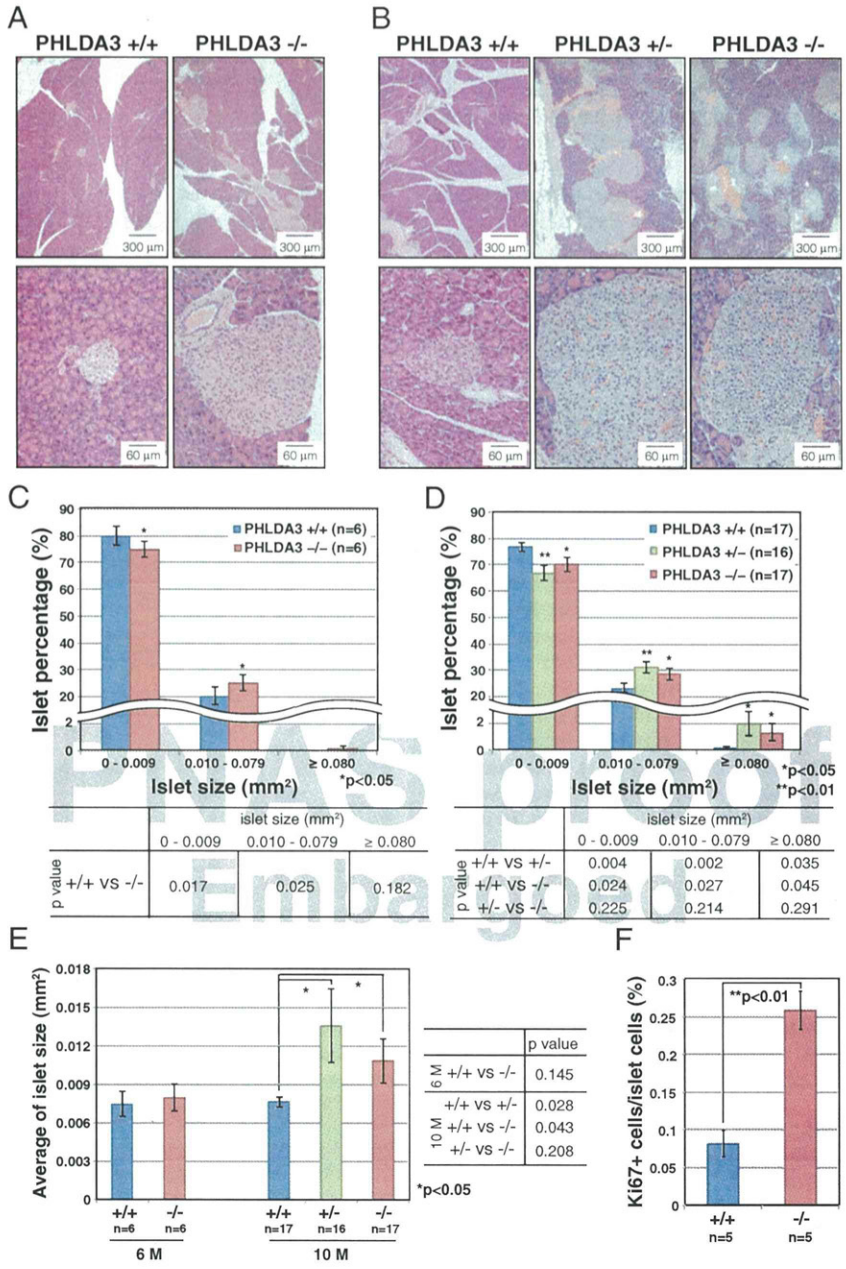

Fig. 6. Hyperplastic islets in *PHLDA3*-deficient mice. Six-month-old (21- to 31-wk-old) (*A*, *C*, and *E*) and 10-mo-old (39- to 49-wk-old) (*B* and *D*–*F*) mice were analyzed. (*A* and *B*) Hematoxylin and eosin staining of islets from wild-type, heterozygote and *PHLDA3*-deficient mice (*A*, 6-mo; *B*, 10-mo). (*C*–*E*) Calculation of islet sizes. Islet areas were calculated from hematoxylin and eosin-stained pancreas sections. One (6-mo-old mice) or three pancreas sections (10-mo-old mice; sections separated by more than 20 μm *z* axis) were analyzed per mouse. Islet areas from indicated numbers (n) of mice were analyzed. Size distributions of islets (*C*, 6-mo; *D*, 10-mo) and average islet sizes (*E*; 6- and 10-mo-old) are shown. The *P* values between $PHLDA3^{+/+}$ and $PHLDA3^{+/-}$ or $PHLDA3^{-/-}$ were calculated and are shown (**P* < 0.05; ***P* < 0.01). (*F*) Quantitation of Ki67-positive cells. Pancreas sections from indicated numbers (n) of mice were analyzed. Islet nuclei number and Ki67-positive nuclei number were counted and the percentage of Ki67-positive cells was calculated. (***P* < 0.01) Representative images are shown in *SI Appendix*, Fig. S4.

of β and α cells, respectively, within the islets. Normal murine islets have β cells in the center of the islet and α cells at the periphery surrounding the β cells (as shown in $PHLDA3^{+/+}$ islets in Fig. 7*A*). However, in the hyperplastic islets of $PHLDA3^{+/-}$ and $PHLDA3^{-/-}$ mice, huge numbers of β cells and relatively small numbers of α cells were often observed, and the hyperplastic islets often showed abnormal islet architecture, with few α cells at the periphery of the islets (Fig. 7*A*). We calculated the areas occupied by α and β cell types to determine which of these had increased. As shown in Fig. 7*B*, the mean percentage area occupied by β cells was significantly higher in $PHLDA3^{-/-}$ islets. The area occupied by β cells was also significantly high in large $PHLDA3^{-/-}$ islets (larger than 0.05 mm^2) compared with that seen in large islets infrequently found in $PHLDA3^{+/+}$ mice (Fig. 7*B*). Because we had found a significantly higher number of proliferating cells in $PHLDA3^{-/-}$ islets (Fig. 6*F*), we stained the islets with anti-Ki67, -insulin, and -glucagon antibodies to identify which cell types within the islets were proliferating. As shown

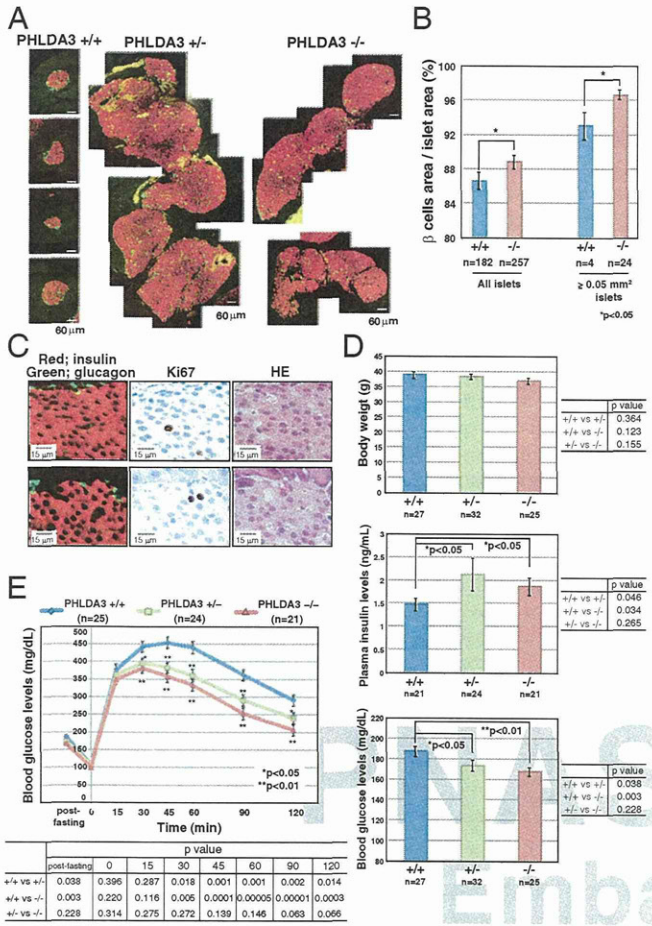

	p value						
	post-fasting	0	15	30	45	60	90	120
+/+ vs +/-	0.038	0.396	0.287	0.018	0.001	0.001	0.002	0.014
+/+ vs -/-	0.003	0.220	0.116	0.005	0.0001	0.00005	0.00001	0.0003
+/- vs -/-	0.228	0.314	0.275	0.272	0.139	0.146	0.063	0.066

Fig. 7. Proliferation of β cells in the islets of *PHLDA3*-deficient mice. Ten-mo-old (39- to 49-wk-old) mice were analyzed. (*A*) Distribution of β and α cells in pancreas sections. Pancreas sections were stained with antibodies to identify β cells (anti-insulin; red) and α cells (anti-glucagon; green). Representative images of hyperplastic islets from $PHLDA3^{+/-}$ and $PHLDA3^{-/-}$ mice are shown. (*B*) Percent area occupied by β cells. Pancreas sections were stained as in *A*, and areas occupied by α- and β-cells in indicated numbers of islets from $PHLDA3^{+/+}$ (five mice were analyzed) and $PHLDA3^{-/-}$ (six mice were analyzed) were calculated and percentages of β-cell areas in the islets were determined. Semihyperplasic islets and hyperplastic islets (larger than 0.05 mm^2 islet area) were separately calculated and shown at the right. (*P < 0.05; **P < 0.01). (*C*) Proliferation in pancreas sections. Serial pancreas sections of $PHLDA3^{-/-}$ mice were stained with anti-insulin and anti-glucagon, anti-Ki67 and HE, to determine the cell types that are Ki67 positive. Representative images are shown. (*D*) Body weight, blood glucose and insulin levels. Indicated numbers (n) of mice were analyzed. Plasma insulin levels and blood glucose levels were determined in blood from tail vein samples, and were determined twice for each mouse. Mice were fed ad libitum. (*P < 0.05; **P < 0.01). (*E*) Glucose tolerance test (GTT). Indicated numbers (n) of overnight-fasted mice were subjected to GTT by i.p. injection of glucose (2 mg/g body weight). GTT was performed twice for each mouse. The P values between $PHLDA3^{+/+}$ and $PHLDA3^{+/-}$ or $PHLDA3^{-/-}$ were calculated and are shown in the panels (*P < 0.05; **P < 0.01). The differences between $PHLDA3^{+/-}$ and $PHLDA3^{-/-}$ were not significant (P > 0.05).

in Fig. 7*C*, we found that most Ki67-positive cells were β cells in $PHLDA3^{-/-}$ islets. Taken together, these data show that islet β cell proliferation is enhanced in *PHLDA3*-deficient islets.

It would be expected that abnormal proliferation of β cells would result in the excess production of insulin, leading to altered glucose metabolism in *PHLDA3*-deficient mice. As shown in Fig. 7*D*, although the *PHLDA3* genotype had no influence on body weights, 10-mo-old $PHLDA3^{+/-}$ and $PHLDA3^{-/-}$ mice had higher plasma insulin and lower blood glucose levels compared with age-matched wild-type mice under fed conditions. Similar results were obtained in 6-mo-old fed mice (*SI Appendix*, Fig. S9*A*) and in 10-mo-old fasted mice (*SI Appendix*, Fig. S9*B*). Therefore, we performed glucose tolerance tests and found significant enhancement of glucose tolerance in $PHLDA3^{+/-}$ and $PHLDA3^{-/-}$ mice (Fig. 7*E*). These data show that loss of PHLDA3 expression results in enhanced proliferation of islet cells, especially β cells, and consequential increase of insulin secretion.

We further characterized $PHLDA3^{-/-}$ islets using several β cell markers: the endocrine cell marker chromogranin A (*SI Appendix*, Fig. S10), the β cell differentiation marker Glut2 (*SI Appendix*, Fig. S11), and deposition of IAPP (islet amyloid polypeptide; *SI Appendix*, Fig. S12). None of these markers showed significant difference compared with $PHLDA3^{+/+}$ islets, indicating that $PHLDA3^{-/-}$ islets retain normal β cell characteristics, to the extent we examined.

***PHLDA3*-Deficient Islets Have Enhanced Akt Activity and Larger Cell Size, and Are Resistant to Apoptosis.** We further analyzed the effects of PHLDA3 deficiency on several Akt-regulated biological processes. We first confirmed reduction or loss of *PHLDA3* expression in $PHLDA3^{+/-}$ and $PHLDA3^{-/-}$ mice islets (Fig. 8*A*). We found that activation of Akt and phosphorylation of its downstream molecules were augmented in $PHLDA3^{-/-}$ islets (Fig. 8*B*). It has been reported that enhanced Akt activity has an effect on islet cell size (5, 6). We therefore analyzed islet cell size in $PHLDA3^{+/+}$, $PHLDA3^{+/-}$, and $PHLDA3^{-/-}$ mice. As shown in Fig. 8*C*, islet cell size was significantly increased in $PHLDA3^{-/-}$ and $PHLDA3^{+/-}$ mice. We next analyzed the sensitivity of $PHLDA3^{-/-}$ islets to apoptosis. Wild-type or $PHLDA3^{-/-}$ mice were treated with STZ for 5 consecutive days to produce β cell injury. It is known that STZ-induced apoptosis of β cell results in the elevation of blood glucose, and can thereby experimentally induce type I diabetes in mice. We analyzed blood glucose levels at the indicated times following STZ treatment, and STZ administration resulted in the effective elevation of blood glucose levels in wild-type mice, whereas elevation was diminished in $PHLDA3^{-/-}$ mice (Fig. 8*D*). When we calculated β cell and α cell areas in STZ-treated mice, we observed a significant increase in the area occupied by β cells in *PHLDA3*-deficient mice, showing that PHLDA3 is required for the efficient induction of β cell apoptosis by STZ (Fig. 8*E*). These results demonstrate that PHLDA3 controls Akt activity, cell size, and apoptosis of islet cells in vivo.

Discussion

In this report, we have shown that PHLDA3 is a candidate tumor suppressor in PanNETs. We observed that the LOH of the *PHLDA3* gene locus in human PanNETs occurs at a remarkably high frequency and is comparable to that of the *MEN1* gene locus, the gene reported to be most frequently affected in PanNETs (15). We also showed that LOH at the *PHLDA3* gene locus is associated with disease progression and poor prognosis in PanNETs. In contrast, LOH/mutation of *MEN1* was found to be unrelated to the prognosis of PanNET patients, both in this and in a previous study (7). These results show that the PHLDA3-regulated tumor suppression pathway is relevant to the progression and malignant phenotype of PanNETs and the poor prognosis of PanNET patients. Because PHLDA3 is a repressor of Akt, we propose that inhibition of the Akt pathway would improve the prognosis of PanNET patients exhibiting LOH of *PHLDA3*. This possibility is supported by the reported clinical efficacy of the Akt pathway inhibitor Everolimus, which has been shown to improve the survival of PanNET patients significantly. Everolimus treatment was approved in Japan only from 2011, and therefore none of the patients in our study had received Everolimus. We speculate that patients who are positive

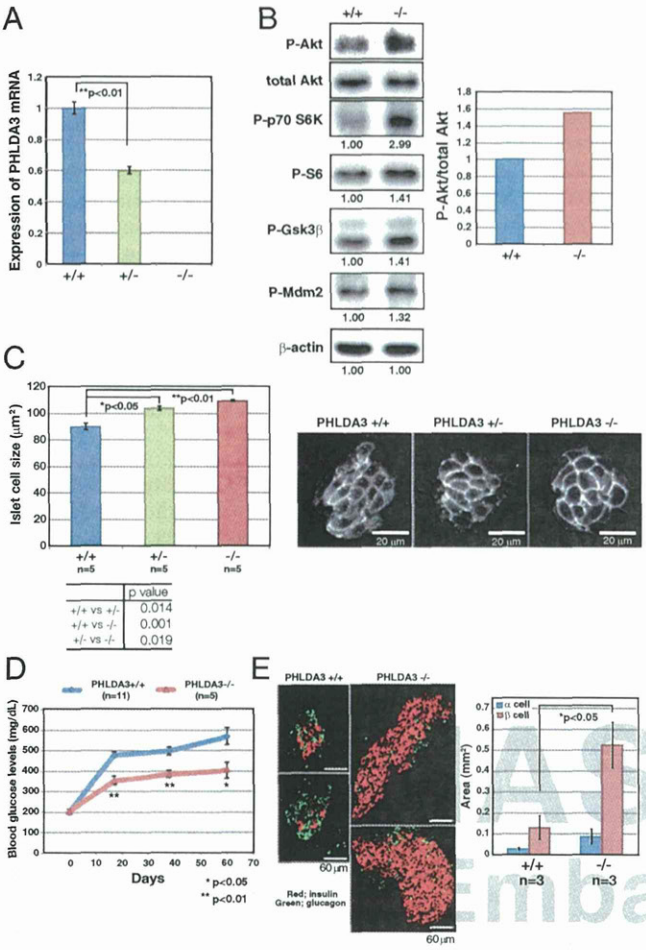

Fig. 8. Akt activation in islets of *PHLDA3*-deficient mice. (*A*) *PHLDA3* mRNA expression in isolated islets. Islets were isolated from $PHLDA3^{+/+}$, $PHLDA3^{+/-}$, and $PHLDA3^{-/-}$ mice, and analyzed for *PHLDA3* expression by quantitative RT-PCR, normalized to β-actin. (*B*) Akt activity and phosphorylation of Akt downstream signaling molecules in isolated islets. Akt activation and phosphorylation of Akt downstream signaling molecules were analyzed by Western blotting and quantified by normalization to total Akt levels (P-Akt, *Right*) or by β-actin levels (P-p70 S6K, P-S6, P-GSK3β, and P-Mdm2). (*C*) Islet cell size in *PHLDA3*-deficient mice. (*Left*) Indirect immunofluorescence staining of Glut2 in pancreas section from 10-mo-old mice. (*Right*) Islet areas and nuclei numbers were calculated, and mean islet cell sizes were determined from one hematoxylin- and eosin-stained pancreas sections per indicated numbers (n) of mice. The *P* values between $PHLDA3^{+/+}$ and $PHLDA3^{+/-}$ or $PHLDA3^{-/-}$ were calculated and shown in the panels (*$P < 0.05$; **$P < 0.01$). The difference between $PHLDA3^{+/-}$ and $PHLDA3^{-/-}$ was also significant ($P < 0.05$). (*D*) Blood glucose levels in streptozotocin-induced diabetic mice. Indicated numbers (n) of $PHLDA3^{+/+}$ or $PHLDA3^{-/-}$ mice were injected i.p. with STZ for 5 consecutive days. Blood glucose levels were determined at different time points as indicated after administration of STZ. (*$P < 0.05$; **$P < 0.01$). (*E*) Distribution of β and α cells in STZ-treated $PHLDA3^{+/+}$ and $PHLDA3^{-/-}$ mice. (*Left*) Sections were stained with antibody against insulin (β cell marker; red) and glucagon (α cell marker; green) and representative images are shown. Pancreas sections of three $PHLDA3^{+/+}$ and three $PHLDA3^{-/-}$ mice were analyzed. (*Right*) For each mouse, α-cell and β-cell areas were calculated from one pancreas section. (*$P < 0.05$.)

for *PHLDA3* LOH and have a poor prognosis may benefit most from Everolimus treatment. Furthermore, determination of *PHLDA3* LOH status could serve as a diagnostic measure to select patients who should receive Everolimus. Thus, it will be important to conduct a prospective study to analyze the effect of Everolimus in patients with or without *PHLDA3* LOH.

We have shown that PHLDA3 regulates Akt activity and various Akt-regulated biological processes, i.e., cell proliferation, cell size, and apoptosis, in cultured cell lines and in vivo endocrine cells. Several laboratories have generated transgenic mice that specifically express active Akt in β cells (6, 16). These mice developed hyperplastic islets, but did not develop malignant PanNETs (17). Likewise, we have shown that loss of PHLDA3 and the resulting activation of Akt leads to hyperplastic islet development, but not to the development of PanNETs. Although Akt activation is observed in various cancers and contributes to tumorigenesis and tumor progression, the conclusion derived from these experiments is that activation of Akt pathway alone is insufficient to cause PanNETs unless combined with an oncogenic event in a second pathway. In human PanNETs, double LOH of *PHLDA3* and *MEN1* is frequently observed. In these cells, loss of PHLDA3 function, i.e., activation of Akt, is combined with loss of MEN1 function to promote PanNET tumorigenesis, and loss of PHLDA3 function particularly contributes to the progression of PanNETs. It would therefore be interesting to generate mice that are doubly deficient in *PHLDA3* and *MEN1* to analyze whether the islet phenotypes are more pronounced and the hyperplastic islets more prone to malignancy.

We observed hyperplastic islets in *PHLDA3* heterozygote (+/−) mice as well as *PHLDA3*-deficient (−/−) mice. This observation suggests that *PHLDA3* is haplo-insufficient for the suppression of endocrine cell proliferation. We have previously shown that PHLDA3 expression represses Akt activity in a dose-dependent manner, consistent with the possibility that loss of a single *PHLDA3* allele could lead to enhanced Akt activation and enhanced proliferation of endocrine cells (8). However, we have also shown that in human PanNETs, the *PHLDA3* locus undergoes methylation in addition to LOH, suggesting that two hits on the *PHLDA3* gene is required for human PanNET development. We assume that loss of both *PHLDA3* alleles, and consequent stronger activation of Akt, may be required to exert a tumorigenic phenotype. Future studies should examine the islet phenotypes of $PHLDA3^{+/-}$ and $PHLDA3^{-/-}$ in a $MEN1^{-/-}$ background. We expect that, in a $MEN1^{-/-}$ background, $PHLDA3^{-/-}$ mice would develop PanNETs more frequently than in $PHLDA3^{+/-}$ mice. In addition, because we found association of LOH at the *PHLDA3* locus in both nonfunctional and functional human PanNETs, whether nonfunctional PanNETs develop in these mice is an interesting issue.

We previously identified *PHLDA3* as a p53 target gene. In the present study, we show that the *PHLDA3* locus undergoes frequent LOH in PanNETs, a tumor type in which p53 mutations are rare (3, 7). Recently it has been reported that among the various target genes of p53, *PHLDA3* displays prominent tumor suppressor activity (18). Therefore, in tumors harboring a p53 mutation, loss of p53-regulated *PHLDA3* expression may significantly contribute to tumor progression, whereas in tumors without a p53 mutation, loss of the *PHLDA3* gene itself may drive oncogenesis. Interestingly, global methylation profiling of prostate cancer specimens has revealed significant methylation of the *PHLDA3* gene in these cancers (19). In addition, in the COSMIC database, 11 PHLDA3 mutations in several cancers are reported. All mutations are located within the PH domain of PHLDA3, and nonsynonymous mutations may result in loss of Akt repressing ability. Therefore, in addition to inactivation by methylation, these and other mutations that result in a functional loss of PHLDA3 may contribute to some cancers.

In summary, our results show that PHLDA3 is a novel tumor suppressor of PanNET, and PHLDA3 and MEN1 cooperatively suppress its development. PHLDA3 represses Akt activity in islet cells and hyperplastic islets are found in both $PHLDA3^{+/-}$ and $PHLDA3^{-/-}$ mice. Collectively, our data illustrates the importance of the PHLDA3-regulated tumor suppression pathway in PanNETs.

Materials and Methods

Cell Lines, Cell Culture, Transfection, Adenovirus Infection, and Soft Agar Colony Formation Assay. Cell lines used in this study were: LNCaP (human prostate cancer), MDA-MB-M468 (human breast cancer), DLD1 (human colorectal cancer), H1299 (human lung NET), A99 (human PanNET, ref. 20), RIN (rat pancreatic β cell), and MIN6 (mouse pancreatic β cell). Cell culture and transfection was performed as described (21). The siRNAs were introduced using RNAiMAX (Invitrogen). ON-target plus control and ON-target plus PHLDA3-targeting siRNAs were purchased from Dharmacon Research. Adenovirus infection was performed using previously described adenoviruses expressing LacZ or N-terminally HA-tagged PHLDA3 (8). Everolimus (AdooQ BioScience) was added to cultures at the indicated concentrations. For soft agar colony formation assays, cells were seeded in 3-cm dishes with a bottom layer of 0.5% agarose and a top layer of 0.33% agarose, both in complete media. The assay was performed in triplicate for each sample. Colonies were photographed after 9 (H1299) or 10 (MIN6) days of incubation. Colonies were counted in three to five different views from each plate to calculate average values. The total numbers of colonies larger than 100 (MIN6) or 200 (H1299) pixels were counted per view.

Western Blotting Analysis. Cells were lysed in lysis buffer [50 mM Tris·HCl (pH 8.0), 1% Nonidet P-40, 250 mM NaCl, 50 mM NaF, 1 mM Na_3VO_4, 1 mM protease inhibitor (PMSF, aprotinin, leupeptin) and 1 mM DDT]. Whole cell lysates were subjected to protein quantification and analyzed by Western blotting. To detect PHLDA3, 20 μg of whole cell lysates (WCL) were loaded. To detect other proteins, 5 μg of WCL were loaded. Antibodies used in this study were: anti-Akt rabbit polyclonal antibody, anti-phospho-Akt (S473) rabbit monoclonal antibody, anti-p70S6K rabbit monoclonal antibody, anti-phospho-p70S6K (T389) rabbit polyclonal antibody, anti-phospho-S6 (S240/244) rabbit monoclonal antibody, anti-phospho-Gsk3β (S9) rabbit polyclonal antibody, anti-phospho-Mdm2 (S166) rabbit polyclonal antibody from Cell Signaling Technology, anti-actin mouse monoclonal antibody from SIGMA from Santa Cruz Biotechnology, anti-PHLDA3 goat polyclonal antibody from Abcam, anti-HA monoclonal antibody (clone 12CA) from Roche Diagnostics.

Reverse Transcription and Real-Time PCR. Reverse transcription was carried out using kits from Invitrogen following the manufacturer's instructions (SuperScript First-Strand Synthesis System for RT-PCR). Total RNA (0.2–5 μg) was used for reverse transcription. Reverse-transcribed cDNAs were subjected to real-time PCR, which was performed with a LightCycler 480 Instrument (Roche Diagnostics). For the detection of PHLDA3 (human; Hs00385313_m1, mouse; Mm00449846_m1, rat; rat; Rn01483684_m1), beta actin (mouse; Mm00607939_s1, rat; Rn00667869_m1) and GAPDH (human; Hs02758991_g1, mouse; Mm99999915_g1), TaqMan probe from Applied Biosystems was used.

BrdU Incorporation Assay and Measurement of Cell Number. BrdU-positive cells were quantified using the Ziva Ultrasensitive BrdU assay (Jaden BioScience). This assay detects the incorporation of BrdU using a labeled anti-BrdU antibody and detection substrate in an ELISA format. By this assay, a small fraction of proliferating cells within a large population of nonproliferating cells can be detected. Cell numbers were analyzed by using CellTiter-Glo Luminescent Cell Viability Assay (Promega). Using this assay, viable cells are determined by quantitation of ATP, an indicator of metabolically active cells.

Flow Cytometry and TUNEL Assay. Apoptosis of islet cells was quantitated by the TUNEL reaction using the In Situ Cell Death Detection kit, Fluorescein (Roche Diagnostics) followed by flow cytometry. Flow cytometry analysis was performed using a FACS Calibur instrument (Becton Dickinson).

Tumor Samples Used in the Study, and DNA and RNA Extraction from Primary Tumor Samples. The tumor samples used in this study were surgically resected at the National Cancer Center Hospital (44 samples; PanNET1-18, 24–47, 52, 53), Kyotc University Hospital (6 samples; PanNET19-23, 51), or Kagawa University Hospital (4 samples; PanNET 48–50, 54) between 1993 and 2012. This study was approved by the Institutional Review Board of the National Cancer Center, Tokyo. Clinical and pathological data were obtained through a detailed retrospective review of the medical records of all patients with PanNET. Five-micrometer sections of paraffin-embedded tissues were subjected to DNA extraction. Total RNA was extracted from frozen normal pancreas and tumor samples using an RNeasy mini kit (Qiagen).

Microsatellite Analysis. Microsatellite analysis was performed basically as described (8). We used six primer pairs labeled with FAM that amplify microsatellite loci to achieve accurate detection of LOH at the *PHLDA3* locus (Fig. 1*A*). For the *MEN1* locus, three primer pairs were used (Fig. 2*A*). Amplified PCR products were analyzed with a 3100 automated sequencer (Applied Biosystems). Collected data were analyzed with GeneScan and Genotyper software (Applied Biosystems), and allele sizes and peak heights were calculated. The genotype was determined to be heterozygous if two bands of different sizes were obtained from normal tissues. A ratio of the two peaks in tumor DNA of less than 0.7 in comparison with the corresponding ratio of the two peaks in nontumor DNA was considered as allelic loss.

5-aza-dC Treatment and Methylation-Specific PCR. Cells were seeded at a density of 3×10^5 cells (H1299 and A99) or 3×10^6 (MIN6) cells per 10-cm dish on day 0 and treated with freshly prepared 5-aza-dC (Sigma-Aldrich) for 24 h on days 1, 3, and 5. After each treatment, cells were placed in fresh medium and harvested on day 6. Genomic DNA was extracted and subjected to bisulfite conversion using EZ DNA Methylation kit (Zymo research). Fully methylated controls were prepared by methylating genomic DNA with SssI methylase (New England Biolabs). Methylation-specific PCR (MSP) was performed basically as described (22). MSP was performed using the specific primer sets shown below. BS-F and R primers were used to amplify DNA with or without methylation. MSP-F and R primers were used to amplify methylated DNA.

BS-F: GTAGATAGAGTTTAGGGGAGTAAGAG

BS- R: CTCTACCCCAACTAACCCAACCC

MSP-F: GAGGGTTGGTTAGGGTAGGAATGTG

MSP-R: ACTCCCCTAAACTCTATCTACACAC

Mice Used in This Study. Generation of *PHLDA3*-deficient mice was reported (23). Briefly, a *PHLDA3*neo targeting vector was obtained by cloning a 6-kb upstream KpnI fragment and a 6-kb downstream HindIII/NotI fragment into pPNT1. The resulting deletion (nucleotides 579–2,096 of GenBank accession no. AF151099) eliminates all of exon 1 and part of exon 2, thus deleting the entire *PHLDA3* coding region. *PHLDA3*$^{-/-}$ mice were generated by crossing the heterozygotes. MEFs were isolated and maintained as described (24). Mouse experiments were performed in a specific pathogen-free environment at the National Cancer Center animal facility according to institutional guidelines, and all of the animal experiments were approved by the Committee for Ethics in Animal Experimentation at the National Cancer Center.

Blood Glucose, Plasma Insulin Measurement, and Glucose Tolerance Tests. Blood glucose levels were determined with blood samples from tail vein punctures in mice using Glucose pilot (Aventir Biotech), according to the procedures specified by the manufacturer. Plasma insulin levels were determined with blood samples from tail vein punctures or inferior vena cava in mice by ELISA (Morinaga Institute of Biological Science), according the procedures specified by the manufacturer. For glucose tolerance tests, mice were fasted overnight and blood was drawn from tail vein at 0, 15, 30, 45, 60, 90, and 120 min after i.p. injection of D-glucose (2 mg/g of body weight).

Quantitative Measurement of Islet Morphology. Islet area and islet nuclei number were measured from hematoxylin and eosin-stained pancreas sections and Ki67-positive cells were counted from immunohistochemically stained pancreas sections using TissueFAXS (TissueGnostics). Chromogranin A signal intensity was also measured using TissueFAXS. α and β cells areas were quantified by the number of pixels in each immunohistochemically stained area in images taken by fluorescence microscopy (Olympus IX2-DSU).

Isolation of Rat and Mouse Primary Islets and Preparation of Primary Islet Cells. The animal experiment was reviewed and approved by the Institutional Animal Care and Use Committee for Frontier Medical Sciences, Kyoto University. For isolation of rat islets, Lewis or Wistar rats (male, aged 9–11 wk, Shimizu Laboratory Supplies) were used. Islet isolation was performed according to previously described methods (25). Briefly, through midline laparotomy, 10 mL of a type XI collagenase solution (1200 CDU/mL, C9407, Sigma-Aldrich) was infused into the common bile duct that was ligated at the hepatic side before the inflow into the duodenum. The pancreases were removed and digested in a water bath set at 37 °C for 18 min. The digested pancreases were filtered with a stainless steel sieve to separate the islets, and purified using a discontinuous gradient solution (Dextran 70, 17–0280-02, Amersham). Mouse islets were isolated from 10- to 25-wk-old male animals by collagenase digestion of the pancreas, followed by purification using a Ficoll gradient. Islets were handpicked twice. The harvested islets

were cultured in RPMI or CRML-1066 medium (11530, Gibco) supplemented with a 1% antibiotic–antimycotic solution (15240-062, Gibco) and 10% FBS (12103-78P, JRH) in an incubator set at 5% CO_2, 37 °C.

Primary islet cells were prepared by digesting the islets with Accutase for 15 min at 37 °C. Islet cells were washed with RPMI before use in experiments.

Immunohistochemistry. Immunohistochemistry (IHC) was performed basically according to the manufacturer's instructions. In brief, after deparaffinization, tissues sections underwent antigen retrieval by autoclaving slides for 5 min in 10 mM citrate buffer (pH 6.0). For fluorescent immunohistochemical staining of insulin, glucagon, and Glut2, nonspecific interactions were blocked for 30 min using a 5% goat serum solution. The primary antibodies were: guinea pig anti-insulin polyclonal antibody (Abcam) diluted 1:400, mouse anti-glucagon monoclonal antibody (Sigma-Aldrich) diluted 1:750 and rabbit anti-Glut2 polyclonal antibody (Alpha Diagnostic) diluted 1:750 with Signal Enhancer HIKARI (Nacalai Tesque). These were applied to the slides and incubated overnight at 4 °C. As secondary antibodies, Alexa Fluor 488 goat anti-mouse IgG antibody (Invitrogen) diluted 1:500, Alexa Fluor 488 goat anti-rabbit IgG antibody (Invitrogen) diluted 1:500 and Alexa Fluor 546 goat anti-guinea pig IgG antibody (Invitrogen) diluted 1:1,000 with PBST-BSA were applied to the slides and incubated 3 h at room temperature. To detect Ki67- and Chromogranin A-positive cells, sections were pretreated with 0.3% H_2O_2 for inactivation of endogenous peroxidase. The primary antibody, rat anti-Ki67 monoclonal antibody (DakoCytomation) diluted 1:200, or rabbit anti-Chromogranin A polyclonal antibody (Thermo Scientific) diluted 1:200 with Signal Enhancer HIKARI were applied to the slides and incubated overnight at 4 °C. As secondary antibodies, Histofine Simple Stain MAX PO anti-rat IgG antibody (Nichirei Bioscience) or biotinylated anti-rabbit IgG antibody (VECTOR Laboratories) was used. We used 3,3′-diaminobenzidine tetrahydrochloride (DAB; Muto Pure Chemicals) as the substrate chromogen. The sections were counter stained with hematoxylin.

STZ-Induced Diabetes. Eleven- to 22-wk-old wild-type and *PHLDA3* knockout male mice were injected i.p. with 50 mg/kg streptozotocin daily for 5 consecutive days (Sigma-Aldrich) to produce β cell injury. On days 92, 93, 99, and 100, animals were killed.

Statistical Analysis. Data were calculated and shown as mean ± SD (for Figs. 4, 5, and 9 and *SI Appendix*, Fig. S3) or as mean ± SEM (Figs. 6–8 and *SI Appendix*, Figs. S7, S9, and S10*A*). Comparisons between the samples were performed by Student *t* test. Survival data were analyzed using XLStat software (version 2013.4.05; Addinsoft), and Kaplan–Meyer plots were drawn. Wilcoxon test was performed to assess the statistical significance of the difference between the survival curves. In Fisher's exact test, *P* values were obtained by using two tails. Statistical significance was defined as $P < 0.05$.

ACKNOWLEDGMENTS. We thank T. Niwa and T. Ushijima (National Cancer Center, Japan) for advice on methylation-specific PCR, Marc Lamphier for critical reading of the manuscript, Dr. Wanxing Cui for providing isolated human islets, and Drs. T. Yoshida and H. Sakamoto and National Cancer Center Research Core Facility (supported by National Cancer Center Research and Development Fund, 23-A-7) for the LOH analyses in this study. This study was supported by Grants-in-Aid for Scientific Research from the Ministry of Education, Culture, Sports, Science and Technology of Japan (23501279 and 26430133, to R.O.); New Energy and Industrial Technology Development Organization (NEDO) (09A02012a, to R.O.); research grants from Daiichi-Sankyo Foundation of Life Science (to R.O.); the Ichiro Kanehara Foundation (R.O.); Takeda Science Foundation (R.O.); Astellas Foundation for Research on Metabolic Disorders (R.O.); Foundation for Promotion of Cancer Research in Japan (R.O.); Extramural Collaborative Research Grant of Cancer Research Institute, Kanazawa University, Japan (to R.O.); Cooperative Research Program of Institute for Frontier Medical Sciences, Kyoto University, Japan (R.O.); and grants from the National Cancer Center Research and Development Fund (23-B-9, to R.O.; and 23-A-11, to T.T.).

1. Hauso O, et al. (2008) Neuroendocrine tumor epidemiology: Contrasting Norway and North America. *Cancer* 113(10):2655–2664.
2. Yao JC, et al. (2008) One hundred years after "carcinoid": Epidemiology of and prognostic factors for neuroendocrine tumors in 35,825 cases in the United States. *J Clin Oncol* 26(18):3063–3072.
3. de Wilde RF, Edil BH, Hruban RH, Maitra A (2012) Well-differentiated pancreatic neuroendocrine tumors: From genetics to therapy. *Nat Rev Gastroenterol Hepatol* 9(4):199–208.
4. Yao JC, et al.; RAD001 in Advanced Neuroendocrine Tumors, Third Trial (RADIANT-3) Study Group (2011) Everolimus for advanced pancreatic neuroendocrine tumors. *N Engl J Med* 364(6):514–523.
5. Elghazi L, Bernal-Mizrachi E (2009) Akt and PTEN: Beta-cell mass and pancreas plasticity. *Trends Endocrinol Metab* 20(5):243–251.
6. Tuttle RL, et al. (2001) Regulation of pancreatic beta-cell growth and survival by the serine/threonine protein kinase Akt1/PKBalpha. *Nat Med* 7(10):1133–1137.
7. Jiao Y, et al. (2011) DAXX/ATRX, MEN1, and mTOR pathway genes are frequently altered in pancreatic neuroendocrine tumors. *Science* 331(6021):1199–1203.
8. Kawase T, et al. (2009) PH domain-only protein PHLDA3 is a p53-regulated repressor of Akt. *Cell* 136(3):535–550.
9. Yang YM, et al. (2005) Chromosome 1q loss of heterozygosity frequently occurs in sporadic insulinomas and is associated with tumor malignancy. *Int J Cancer* 117(2): 234–240.
10. Chen YJ, Vortmeyer A, Zhuang Z, Huang S, Jensen RT (2003) Loss of heterozygosity of chromosome 1q in gastrinomas: Occurrence and prognostic significance. *Cancer Res* 63(4):817–823.
11. Corbo V, et al. (2010) MEN1 in pancreatic endocrine tumors: Analysis of gene and protein status in 169 sporadic neoplasms reveals alterations in the vast majority of cases. *Endocr Relat Cancer* 17(3):771–783.
12. Yoo NJ, Kim YR, Lee SH (2011) Expressional and mutational analysis of PHLDA3 gene in common human cancers. *Pathology* 43(5):510–511.
13. Brenet F, et al. (2011) DNA methylation of the first exon is tightly linked to transcriptional silencing. *PLoS ONE* 6(1):e14524.
14. Lenzen S (2008) The mechanisms of alloxan- and streptozotocin-induced diabetes. *Diabetologia* 51(2):216–226.
15. Pannett AA, Thakker RV (1999) Multiple endocrine neoplasia type 1. *Endocr Relat Cancer* 6(4):449–473.
16. Bernal-Mizrachi E, Wen W, Stahlhut S, Welling CM, Permutt MA (2001) Islet beta cell expression of constitutively active Akt1/PKB alpha induces striking hypertrophy, hyperplasia, and hyperinsulinemia. *J Clin Invest* 108(11):1631–1638.
17. Vivanco I, Sawyers CL (2002) The phosphatidylinositol 3-Kinase AKT pathway in human cancer. *Nat Rev Cancer* 2(7):489–501.
18. Brady CA, et al. (2011) Distinct p53 transcriptional programs dictate acute DNA-damage responses and tumor suppression. *Cell* 145(4):571–583.
19. Mahapatra S, et al. (2012) Global methylation profiling for risk prediction of prostate cancer. *Clin Cancer Res* 18(10):2882–2895.
20. Yachida S, et al. (2011) Establishment and characterization of a new cell line, A99, from a primary small cell carcinoma of the pancreas. *Pancreas* 40(6):905–910.
21. Ozeki C, et al. (2011) Cancer susceptibility polymorphism of p53 at codon 72 affects phosphorylation and degradation of p53 protein. *J Biol Chem* 286(20):18251–18260.
22. Yamashita S, Tsujino Y, Moriguchi K, Tatematsu M, Ushijima T (2006) Chemical genomic screening for methylation-silenced genes in gastric cancer cell lines using 5-aza-2′-deoxycytidine treatment and oligonucleotide microarray. *Cancer Sci* 97(1):64–71.
23. Frank D, et al. (2002) Placental overgrowth in mice lacking the imprinted gene Ipl. *Proc Natl Acad Sci USA* 99(11):7490–7495.
24. Ohki R, et al. (2000) Reprimo, a new candidate mediator of the p53-mediated cell cycle arrest at the G2 phase. *J Biol Chem* 275(30):22627–22630.
25. Yang KC, et al. (2010) The cytoprotection of chitosan based hydrogels in xenogeneic islet transplantation: An in vivo study in streptozotocin-induced diabetic mouse. *Biochem Biophys Res Commun* 393(4):818–823.

TSPAN12 is a critical factor for cancer–fibroblast cell contact-mediated cancer invasion

Ryo Otomo[a,b], Chihiro Otsubo[c], Yuko Matsushima-Hibiya[a], Makoto Miyazaki[a,d], Fumio Tashiro[b], Hitoshi Ichikawa[e], Takashi Kohno[f], Takahiro Ochiya[g], Jun Yokota[f], Hitoshi Nakagama[h], Yoichi Taya[i,1], and Masato Enari[a,2]

[a]Division of Refractory Cancer Research, [e]Division of Genetics, [f]Division of Genome Biology, [g]Division of Molecular and Cellular Medicine, and [h]Division of Cancer Development System, National Cancer Center Research Institute, Chuo-ku, Tokyo 104-0045, Japan; [b]Department of Biological Science and Technology, Faculty of Industrial Science and Technology, Tokyo University of Science, Katsushika-ku, Tokyo 125-8585, Japan; [c]Graduate School of Medicine, Kobe University, Chuo-ku, Kobe, Hyogo 650-0017, Japan; [d]Department of Medical Genome Sciences, Laboratory of Tumor Cell Biology, Graduate School of Frontier Sciences, University of Tokyo, Minato-ku, Tokyo 108-8639, Japan; and [i]Cancer Science Institute of Singapore, Centre for Life Sciences, National University of Singapore, 02-07, Singapore 117456

Edited by Moshe Oren, Weizmann Institute of Science, Rehovot, Israel, and accepted by the Editorial Board November 18, 2014 (received for review June 26, 2014)

Communication between cancer cells and their microenvironment controls cancer progression. Although the tumor suppressor p53 functions in a cell-autonomous manner, it has also recently been shown to function in a non–cell-autonomous fashion. Although functional defects have been reported in p53 in stromal cells surrounding cancer, including mutations in the p53 gene and decreased p53 expression, the role of p53 in stromal cells during cancer progression remains unclear. We herein show that the expression of α-smooth muscle actin (α-SMA), a marker of cancer-associated fibroblasts (CAFs), was increased by the ablation of p53 in lung fibroblasts. CAFs enhanced the invasion and proliferation of lung cancer cells when cocultured with p53-depleted fibroblasts and required contact between cancer and stromal cells. A comprehensive analysis using a DNA chip revealed that tetraspanin 12 (TSPAN12), which belongs to the tetraspanin protein family, was derepressed by p53 knockdown. TSPAN12 knockdown in p53-depleted fibroblasts inhibited cancer cell proliferation and invasion elicited by coculturing with p53-depleted fibroblasts in vitro, and inhibited tumor growth in vivo. It also decreased CXC chemokine ligand 6 (CXCL6) secretion through the β-catenin signaling pathway, suggesting that cancer cell contact with TSPAN12 in fibroblasts transduced β-catenin signaling into fibroblasts, leading to the secretion of CXCL6 to efficiently promote invasion. These results suggest that stroma-derived p53 plays a pivotal role in epithelial cancer progression and that TSPAN12 and CXCL6 are potential targets for lung cancer therapy.

cancer-associated fibroblasts | cancer invasion | cancer–stromal cell interaction | p53 | tetraspanin family

The interaction between cancer and stroma plays a key role in tumor progression. Cancer cells alter adjacent stroma to orchestrate a supportive microenvironment. Normal stroma maintains tissue homeostasis, whereas activated stroma promotes tumor growth, angiogenesis, and metastasis, mainly by secreting growth factors, extracellular matrix (ECM) components, and matrix metalloproteinases (1–3). Cancer-associated fibroblasts (CAFs) are representative cells in the cancer microenvironment, and their activity promotes cancer cell proliferation, migration, and invasion (4–6). Tumor growth by prostatic epithelial cells transformed with an SV40-T antigen was greater than that by normal fibroblasts when nude mice were inoculated with CAFs (7).

p53 is a representative tumor suppressor inactivated by mutations or deletions in approximately half of human cancers. It is known as a transcription factor that regulates the expression of genes associated with cell-cycle arrest, apoptosis, and senescence to prevent tumorigenesis (8, 9). However, recent studies suggested that p53 also possessed non–cell-autonomous functions in the interaction between cancer and stromal cells (10, 11). The growth of inoculated cancer cells was more pronounced with the ablation of p53 in host mice (p53 knockout mice) than in p53 intact mice (wild-type mice) (12). A previous study also found that the growth-promoting activity of cancer cells was greater in SCID mice inoculated with cancer cells with p53-deficient fibroblasts than with wild-type fibroblasts (13). Genetic analyses of stromal tissues from cancer patients revealed p53 somatic mutations and the loss of heterozygosity (LOH) in these stromal cells (14–16). p53 expression was also lower in CAFs than in normal fibroblasts (17). Conditioned culture media from cancer cells also inhibited p53 expression in adjacent fibroblasts (18).

Tetraspanin 12 (TSPAN12) belongs to the tetraspanin family, characterized by four transmembrane domains and two extracellular loops (19). Tetraspanin family proteins act as signaling platforms by forming tetraspanin-enriched microdomains, and tetraspanins are involved in the suppression of metastasis (e.g., CD82 and CD9) and tumor progression (e.g., CD151 and TSPAN8) (20–23). Most studies on TSPAN12 have been performed on familial exudative vitreoretinopathy (24, 25), and in vivo functional analyses using TSPAN12-deficient mice revealed that TSAPN12 contributed to retinal vascular development by cooperating with FZD4 and LRP5, and regulated Norrin-induced

Significance

Cancer-associated fibroblasts (CAFs) are abundant and promote cancer proliferation, invasion, and metastasis. Mutations in the p53 gene and decreased p53 expression are often detected in CAFs, and a dysfunction in p53 in CAFs contributes to cancer progression. However, how host-derived p53 influences cancer cells remains unclear. We herein established coculture systems to monitor enhancements in invasiveness and proliferation elicited by p53-depleted fibroblasts and demonstrated that tetraspanin 12 (TSPAN12), identified as a p53-regulated gene, was required for these processes through the contact of cancer cells with stromal fibroblasts and β-catenin–mediated CXC chemokine ligand 6 (CXCL6) secretion. These results suggest that antibodies against TSPAN12 and CXCL6 may be effective therapeutic agents for cancer.

Author contributions: R.O., C.O., and M.E. designed research; R.O., C.O., Y.M.-H., and M.M. performed research; R.O., C.O., H.I., T.K., and M.E. analyzed data; R.O., F.T., T.O., J.Y., H.N., Y.T., and M.E. wrote the paper.

The authors declare no conflict of interest.

This article is a PNAS Direct Submission. M.O. is a guest editor invited by the Editorial Board.

Freely available online through the PNAS open access option.

Data deposition: The data reported in this paper have been deposited in the Gene Expression Omnibus (GEO) database, www.ncbi.nlm.nih.gov/geo (accession no. GSE58753).

[1]Deceased April 16, 2014.

[2]To whom correspondence should be addressed. Email: menari@ncc.go.jp.

This article contains supporting information online at www.pnas.org/lookup/suppl/doi:10.1073/pnas.1412062112/-/DCSupplemental.

β-catenin signaling (26). Furthermore, TSPAN12 has been shown to promote the maturation of tumor-facilitating sheddase ADAM10 (27) and supports human breast cancer growth (28). Thus, TSPAN12 has been suggested to play a role in cancer progression (29).

We herein constructed several coculture assays to elucidate the effects of fibroblasts on cancer cell invasion and proliferation and found that the inactivation of p53 in fibroblasts contributed to cancer cell invasion and proliferation by up-regulating TSPAN12 in fibroblasts. Enhancements in cancer cell invasion and proliferation depended on direct cancer–stromal cell contact and the up-regulation of CXC chemokine ligand 6 (CXCL6) through the TSPAN12–β-catenin pathway.

Results

p53-Depleted Fibroblasts Had Characteristics of Cancer-Associated Fibroblasts. Previous studies using laser-capture microdissected tissue showed that cancer-adjacent stroma had mutations in the p53 gene and LOH in the p53 gene locus (14–16). Therefore, we examined the expression levels of p53 in cancer-associated stromal cells using the Oncomine database (www.oncomine.org). A microarray dataset from the Oncomine database (30) showed that p53 expression was significantly lower in cancer-associated stromal cells than in normal stromal cells (Fig. S1 *A* and *B*). This was consistent with p53 protein levels being lower in cultured CAFs than in normal fibroblasts (17). To address the effects of conditioned media including various factors secreted from lung cancer cells on p53 expression in stromal cells in vitro, human lung fibroblast TIG-7 cells were cultured in conditioned media from lung cancer cells: H1299, A549, and H460 cells, and normal cells: TIG-7 cells and immortalized small airway epithelial cells (SAECs) (Fig. 1*A*). p53 expression in TIG-7 cells was lower when cultured in conditioned media from lung cancer cells than in control media from normal cells (Fig. 1*B* and Fig. S1*C*), which is consistent with the recent finding that the expression of p53 in human lung fibroblast WI-38 cells was decreased by a treatment with conditioned medium derived from cancer cells (18). We then investigated the relationship between p53 and α-smooth muscle actin (α-SMA), a marker of CAFs. The same dataset (30) from the Oncomine database revealed that p53 expression negatively correlated with ACTA2 (α-SMA) expression (Fig. 1*C*). p53 knockdown in fibroblasts increased α-SMA expression, suggesting that the decreased expression of p53 was altered to exhibit CAF-like characteristics (Fig. 1 *D* and *E*).

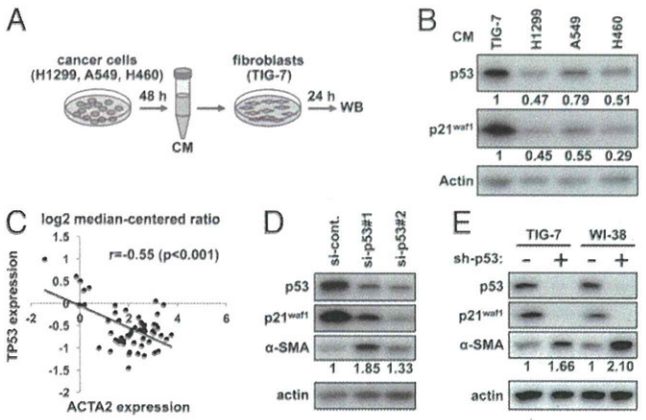

Fig. 1. Down-regulation of p53 in fibroblasts exhibited CAF-like properties. (*A*) Scheme of the experimental design to evaluate p53 expression in TIG-7 cells treated with conditioned media collected from cancer cells. (*B*) p53 expression in TIG-7 cells was down-regulated by conditioned media from cancer cells. TIG-7 cells were treated with conditioned media for 24 h, and expression levels of the indicated proteins in these cell lysates were determined by immunoblotting and quantified using ImageJ version 1.47c software. (*C*) The expression level of α-SMA (ACTA2) negatively correlated with that of p53 (TP53). Expression data were obtained from the Oncomine dataset and plotted to calculate Pearson's product-moment correlation coefficient. $r = -0.55$, $P < 0.001$. (*D* and *E*) The expression level of α-SMA in fibroblasts was up-regulated by p53 knockdown. (*D*) TIG-7 cells were transfected with the indicated siRNAs and, 72 h after transfection, the expression levels of the indicated proteins in these cell lysates were determined by immunoblotting. (*E*) Fibroblasts were infected with either control lentiviruses or lentiviruses for the expression of shRNA against p53. Expression levels of the indicated proteins in these cell lysates were determined by immunoblotting.

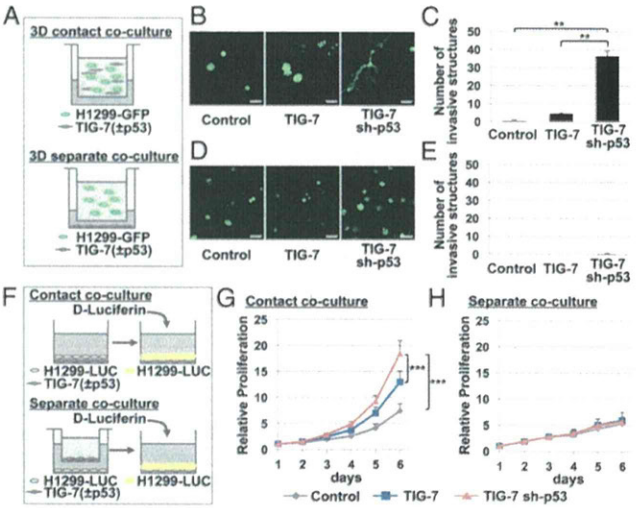

Fig. 2. p53-depleted fibroblasts enhanced invasion and proliferation of cancer cells through direct cell-to-cell contact. (*A*) Scheme of the contact (*Top*) and noncontact (*Bottom*) coculture system using a three-dimensional invasion assay. (*B* and *C*) p53-depleted TIG-7 cells enhanced invasiveness in GFP-labeled H1299 (H1299-GFP) cells using a contact coculture system. H1299-GFP cells were cocultured with parental TIG-7 cells or p53-depleted TIG-7 cells, or cultured alone in Matrigel. After 4–5 d, H1299-GFP cells were observed under a confocal microscope. (Scale bar, 100 μm.) (*B*). Quantification of invasive phenotypic cells in H1299-GFP cells (*C*). (*D* and *E*) p53-depleted TIG-7 cells did not enhance invasiveness in H1299-GFP cells in a noncontact coculture system. H1299-GFP cells were cultured in Matrigel in a Transwell insert, and parental TIG-7 cells or p53-depleted TIG-7 cells were cultured in the bottom well. After 4 or 5 d, H1299-GFP cells were observed under a confocal microscope (*D*). (Scale bar, 100 μm.). Quantification of invasive phenotypic cells in H1299-GFP cells (*E*). (*F*) Coculture systems for cell proliferation assay. Scheme of the contact coculture system using a cell proliferation assay (*Top*). Scheme of the noncontact coculture system using a Transwell insert for cell proliferation assay (*Bottom*). (*G*) p53-depleted TIG-7 cells enhanced proliferation in H1299 cells expressing luciferase (H1299-LUC cells) in a contact coculture system. H1299-LUC cells were cocultured with parental TIG-7 cells or p53-depleted TIG-7 cells, or cultured alone. Luciferase activity was measured every day up to day 6. (*H*) p53-depleted TIG-7 cells did not enhance cell proliferation in H1299-LUC cells using a noncontact coculture system. H1299-LUC cells were cultured in the bottom well, and parental or p53-depleted fibroblasts were cultured in a Transwell insert. Luciferase activity was measured every day until day 6. Data are the mean ± SD of three or more independent experiments. Statistical analyses were performed using the Student *t* test. $^{**}P < 0.01$, $^{***}P < 0.001$.

Cancer Cell Invasion and Proliferation Were Enhanced Through Contact Between Cancer Cells and Fibroblasts. Although the contribution of p53 in fibroblasts to cancer progression has been implied, the underlying molecular mechanism remains unclear. To elucidate the mechanism by which stromal p53 regulates the invasiveness and proliferation of cancer cells, we developed three-dimensional coculture assays using Matrigel. Green fluorescent protein (GFP)-labeled H1299 (H1299-GFP) cells were

mixed with fibroblasts and cocultured in Matrigel, which enabled H1299-GFP cells to directly contact fibroblasts (Fig. 2*A*, *Top*). H1299-GFP cells were then cultured in Matrigel separately from fibroblasts, which enabled them to communicate only through secretions from fibroblasts (Fig. 2*A*, *Bottom*). With direct contact, coculturing H1299-GFP cells with p53-depleted fibroblast TIG-7 cells markedly enhanced the invasiveness of H1299-GFP cells over that of H1299-GFP cells with normal TIG-7 cells (Fig. 2 *B* and *C*). With separation, little or no enhancement was observed in invasiveness in H1299-GFP cells by culturing with fibroblasts, regardless of p53 expression in fibroblasts (Fig. 2 *D* and *E*). Increases in cancer cell numbers also had a negligible effect on cancer invasiveness (Fig. S2 *A–C*), indicating that enhancements in invasiveness were not due to increases in cancer cell numbers in the top chamber. The migration assay showed that a contact coculture with p53-depleted fibroblasts moderately enhanced cancer cell migration over that with controls (Fig. S2 *D–F*), and no significant difference was noted in cell motility under separate coculture conditions (Fig. S2 *G–I*). These results implied that direct contact between cancer cells and stromal fibroblasts was important for cancer cell invasion elicited by stromal fibroblasts when p53 expression levels decreased. We established a coculture system using H1299 cells expressing firefly luciferase (H1299-LUC cells) to assess the effects of fibroblasts on the proliferation of cancer cells. In the direct contact coculture assay, H1299-LUC cells were seeded on TIG-7 monolayer cells and luciferase activity was measured as an indicator of cell proliferation (Fig. 2*F*, *Top*). The rate of proliferation of H1299-LUC cells was greater in a coculture with p53-depleted TIG-7 cells than with H1299-LUC cells alone or with parental TIG-7 cells (Fig. 2*G*). We examined two different approaches as noncontact coculture assays using cell culture inserts to separate each cell (Fig. 2*F*, *Bottom*) and conditioned media from TIG-7 cells (Fig. S3*A*). No significant differences were observed in the rate of proliferation of H1299-LUC cells when cultured with p53-depleted TIG-7 cells or with parental fibroblasts (Fig. 2*H*). The treatment of H1299-LUC cells with conditioned media from p53-depleted TIG-7 cells resulted in a similar rate of cell proliferation to that of H1299-LUC cells with parental TIG-7 cells (Fig. S3*B*). These results suggested that cancer-fibroblast cell contact was required to increase the rate of cancer cell proliferation by coculturing with p53-depleted fibroblasts.

TSPAN12 Was a Derepressive Gene with p53 Ablation. To elucidate the mechanisms responsible for cancer cell invasion and proliferation due to the down-regulation of p53 in fibroblasts, we performed a comprehensive analysis using mRNAs from p53-depleted fibroblasts and control fibroblasts. Microarray experiments showed that 51 genes were up-regulated (fold change, >3) and 9 genes were down-regulated (fold change, <0.33) in p53-depleted fibroblasts (Fig. S4*A*). Of the up-regulated genes, we extracted those that encoded cell-surface proteins because antibodies against such proteins were expected to be candidates for cancer therapy (Fig. S4*B* and Table S1). We also selected and focused on the TSPAN12 gene encoding the tetraspanin family protein that contributes to cancer progression as a less characterized gene from those encoding cell-surface proteins because the induction of TSPAN12 expression in TIG-7 fibroblasts by p53 knockdown was highly reproducible and confirmed that the expression level of TSPAN12 was derepressed in p53-depleted TIG-7 fibroblasts using qRT-PCR and immunoblotting (Fig. 3 *A* and *B*). TSPAN12 was also derepressed by transient p53 knockdown, suggesting that p53 directly regulated TSPAN12 expression (Fig. S4*C*). p53 knockdown in WI-38 fibroblasts also derepressed TSPAN12 expression (Fig. 3 *A* and *B*). We subsequently analyzed TSPAN12 expression in cancer-associated stromal tissues from cancer patients using the Oncomine database (30), and found that TSPAN12 expression was higher in cancer-associated stromal tissues than in stromal tissues from noncancerous regions (Fig. S4 *D* and *E*).

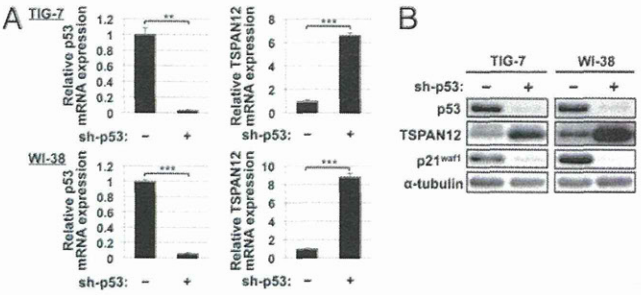

Fig. 3. TSPAN12 was derepressed by p53 knockdown. (*A* and *B*) p53 knockdown derepressed TSPAN12 expression. Total RNAs were prepared from the indicated fibroblasts and expression levels of the indicated genes were subjected to qRT-PCR (*A*). Cell lysates were prepared from the indicated fibroblasts and expression levels of indicated genes were determined by immunoblotting (*B*). Data are the mean ± SD of three or more independent experiments. Statistical analyses were performed using the Student *t* test. $^{**}P < 0.01$, $^{***}P < 0.001$.

Cancer Cell Invasiveness and Proliferation Elicited by p53-Depleted Fibroblasts Were Inhibited by TSPAN12 Knockdown in p53-Depleted Fibroblasts. We determined whether TSPAN12 expression in fibroblasts enhanced cancer cell invasiveness and proliferation. The expression of p53 and TSPAN12 in p53-depleted TIG-7 cells transfected with control siRNAs or siRNAs targeted against TSPAN12 was confirmed by qRT-PCR (Fig. S5*A*) and immunoblotting (Fig. S5*B*), and TIG-7 cells transfected with these siRNAs were cocultured with H1299-GFP cells in Matrigel (Fig. 4*A*). An invasion assay using Matrigel showed that cancer invasiveness elicited by p53-depleted fibroblasts was inhibited by TSPAN12 knockdown in p53-depleted fibroblasts (Fig. 4*B*). These results suggested that the derepression of TSPAN12 by p53 knockdown in fibroblasts was a critical step for enhancing cancer invasiveness. We also investigated whether TSPAN12 knockdown in p53-depleted fibroblasts affected the proliferation of cancer cells using a cell-to-cell contact coculture proliferation assay (Fig. 4*C*). The transfection of si-TSPAN12 in p53-depleted TIG-7 cells decreased the proliferation rate of H1299-LUC cells to that when cocultured with parental TIG-7 cells (Fig. 4*D*). However, the effects of TSPAN12 knockdown in p53-depleted fibroblasts on cancer cell migratory activity were weak even though cancer cell migration was moderately inhibited (Fig. S5*C*). TSPAN12 knockdown in normal TIG-7 cells did not affect basal levels of cancer cell invasiveness and proliferation (Fig. S6 *A–C*). In contrast, the ectopic expression of TSPAN12 in normal TIG-7 cells increased cancer cell invasiveness and proliferation (Fig. S6 *D–F*), suggesting that derepressed TSPAN12 was crucial for enhancing the invasiveness elicited by the down-regulation of p53. We then examined the effects of the extracellular loop of TSPAN12 on invasiveness in p53-depleted cells. The large extracellular loop (LEL) of TSPAN12 could inhibit invasiveness up to basal levels (Fig. S6 *G–I*), implying that TSPAN12-LEL may compete with some factors transducing signals for invasion into cells.

Derepression of TSPAN12 in p53-Depleted Fibroblasts Accelerated Tumor Progression. We tested the effects of stroma-derived p53 on tumor growth in vivo. H1299-LUC cells were mixed with TIG-7 cells in Matrigel, inoculated s.c. into the backs of balb/c-nu/nu mice, and tumor growth was measured using an IVIS bioluminescence imaging system (Fig. 5*A*). TIG-7 cells stably expressed shRNAs targeting p53 and TSAPN12, and reductions in the expression levels of these proteins were confirmed by